Original Article

Improved Grid System Control Using Chaotic PSO-Based PR Controller and Modified SEPIC Topology

R. Karthikeyan[1], K. Boopathy[2]

[1,2]*Department of Electrical and Electronics Engineering, Aarupadai Veedu Institute of Technology,
Vinayaka Missions Research Foundation, Tamilnadu, India.*

[1]*Corresponding Author : rrmdkarthikeyan@gmail.com*

Abstract - *To meet the increasing demand for electricity, it is necessary to use both conventional and unconventional power sources. One type of Renewable Energy Source that turns solar radiation into electricity is a PV system. However, a combination of low irradiance and bad weather prevents installed Photovoltaic (PV) sources from being used to their maximum capacity. PV systems connected to the utility grid supply power to the grid or receive power from the grid depending on the demand and availability of solar energy. As a significance, this research offers an MPPT technique based on ANN to acquire PV power quickly and to the maximum amount possible with zero oscillation tracking. Moreover, a modified SEPIC converter is used to increase the voltage from PV reduced switch 21 level Multi Level Inverter (MLI) changes the DC output of PV modules into alternating current with an increased number of output levels that is compatible with the grid. A chaotic Particle Swarm Optimization (PSO) Proportional Resonant (PR) controller is used to control MLI efficiently, leading to improved AC supply and efficient grid synchronization. MATLAB validation demonstrates the intended system's performance, which reveals enhanced converter efficiency with a lower Total Harmonic Distortion (THD) in contrast to state-of-the-art techniques.*

Keywords - ANN MPPT, Chaotic PSO-PR controller, Modified SEPIC, PV system, Reduced switch 21 level MLI.

1. Introduction

With the depletion of fossil fuels, growing environmental concerns, secured energy, growth production, and lower overall costs in power generation-distribution systems due to technological advancements, the energy generation industry demonstrated a strong leaning to use renewable sources over the past 20 years [1]. Due to its many impressive benefits, including its long lifespan, advanced manufacturing process, noiseless and static operations, rising efficiency, falling costs, flexible construction, and access to government support and incentives, photovoltaic energy is becoming more popular as a pure, renewable source of direct current energy produced from sunbeams [2, 3].

PV-grid tied system represents a pivotal evolution in renewable energy technology, capitalizing on the numerous benefits offered by PV technology. By exploring the features that make PV-grid-tied systems a compelling choice, from their extended lifespan and noiseless operations to the flexibility in construction and governmental support, it becomes evident that these systems are at the forefront of a sustainable energy revolution [4, 5]. Central to the optimization of PV systems is the strategic implementation of voltage converters. These converters play a crucial part in enhancing efficiency, reliability, and overall performance in photovoltaic installations. The Buck-Boost converter is suitable for the initial two stages of a photovoltaic grid-connected inverter due to its broad input voltage range. It can lower inductance and boost conversion efficiency, and it has operating solid characteristics without operation mode changes and straightforward control logic.

However, the existing applications' attempts to improve efficiency and switching frequency as well as implement control circuits are seriously hampered by their poor conversion ratio [6]. If the ratio is low, consider using a Cuk-Converter, a special kind of converter that performs both bucks and boost operations when the source input voltage is inverted. As long as both the input and output currents are consistent, the Cuk-converter may increase the power factor. The switches make the Cuk converter very non-linear, but they are unable to regulate voltage and malfunction in short-term scenarios [7].

The traditional boost converter [8] is employed in high step-up scenarios where there are significant current ripples in the power system, leading to conduction losses. Additionally, easy transferring is required to lower transferring loss and enhance performance when high input current is present due to inductance [9]. Many researchers use the SEPIC converter

in situations requiring high static gain. Considering the SEPIC converter to the normal boost converter, the fixed gain value is twice as high.

Additionally, the switching voltage is only half of the output voltage at which the value occurs. Based on the SEPIC converter [10], a high static gain, low switching stress converter is recommended. In comparison to alternative converters, the Modified SEPIC converter proposed results in a lower input inrush current for the inductor, along with a quicker output voltage peak time and settling time.

In PV systems, an appropriate MPPT controller monitors maximum power point under all environmental circumstances. Many MPPT controllers have been proposed over time, such as the Fuzzy Logic Controller (FLC) [11], Incremental Conductance (INC) [12], and enhanced Perturb and Observe (P&O) [13].

The P&O method's control parameter is disturbed by even a tiny variation in the step size. The direction of step size generated by this method is altered depending on the measurement of PV system output power, which is disturbed by changes in either direction. The Hill Climbing-MPPT [14] approach is widely used in PV-MPPT methods due to its simple application and low cost.

Challenges arise when using large duty cycle steps, leading to more oscillation around a Maximum Power Point (MPP) and reduced convergence speed. Conversely, using tiny duty cycle steps presents its own set of challenges. To address this, the proposed technique utilizing the ANN approach modifies the duty to track the possible power out of PV. A lot of research on various MLI topologies is now being conducted in an effort to lower the number of components needed to create Multilevel Inverters. The traditional Cascaded H-Bridge (CHB) MLI serves as the basis for this reduced switch MLI. Therefore, it has all of the benefits of CHB-MLI and will also require fewer components, which will minimize the Multilevel Inverter's size and cost. In MLI, an approach to control is essential for managing the switch activities [15].

The stated Multilevel inverter topology employs fewer power electronics components, and the circuitry required to perform both control strategies is straightforward. Thus, the inverter will have a sturdy build, be less expensive, be small in size, and be suitable for both low and high-voltage applications [16]. This work introduces a 21-level reduced switch MLI topology in an attempt to achieve the same purpose. The following contributions have been made in order to address the previously mentioned research gap:

- Modified SEPIC implementation with ANN-based MPPT system's power conversion process.
- To guarantee the Reduced Switch 21 Level MLI to operate at its best, a Chaotic PSO-PR controller is incorporated.
- The LC Filter implemented in the system removes the harmonics.

2. Proposed Methodology

PV system, a crucial component of the proposed work, uses solar radiation to generate electricity. However, because of changes in temperature and amount of irradiation, PV voltage is not steady. The proposed strategy uses a higher-performing converter known as a modified SEPIC to increase the voltage produced by PV systems. An ANN-based MPPT controller is developed in this work to regulate the converter with the best possible performance.
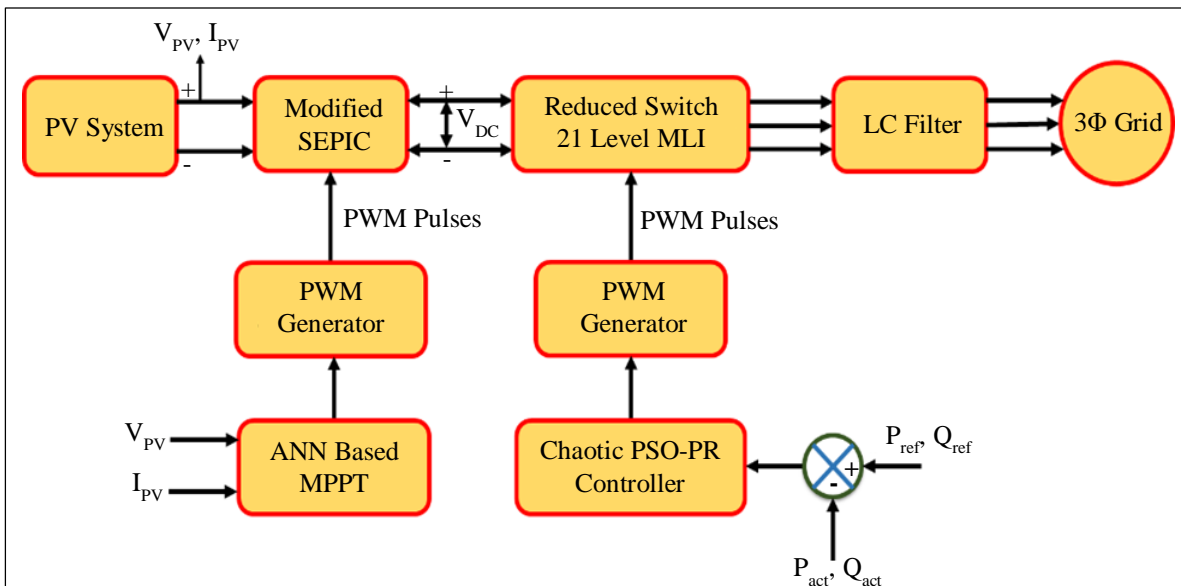

Fig. 1 Proposed model of PV grid system

The controller reacts dynamically to changes in the operating conditions due to its flexibility. This results in a stabilized DC connection voltage, which is then used to convert back into AC using reduced switch 21 level MLI. The implementation of a chaotic PSO-PR controller supports regulating MLI for efficient grid-side functioning. An error signal is produced upon comparison of the real and reactive power. The reduced switch 21 level MLI switches receive the gating pulses produced by the PWM generator. The LC filter receives a stabilized AC supply from MLI, which removes any harmonics from the system and aids in ensuring efficient grid synchronization. Figure 1 presents the block diagram for the proposed system.

3. System Modelling

3.1. Design of PV System

A solar cell connected in parallel and series forms a PV module. A photocurrent generator that mimics the generation of current from light, two resistors in series and parallel that explain the Joule effect and recombination losses, and a p–n junction termed a diode are the three components of a photovoltaic cell.
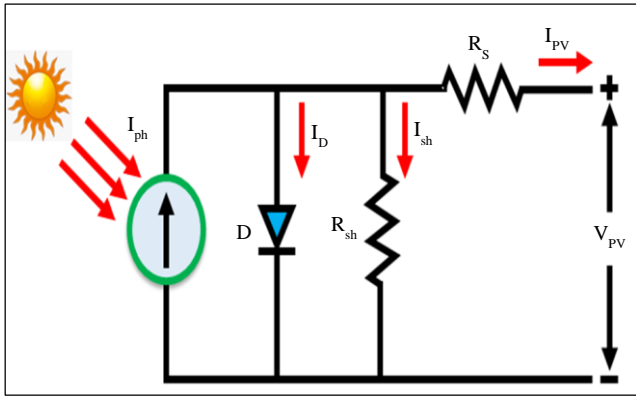

Fig. 2 PV panel equivalent circuit

Using Equation 1 provides the output current according to Kirchhoff's first law. The solar PV gadget is shown as an ideal solar cell with the diode and current source (I_{ph}) in parallel.

$$I = I_{ph} - I_d \tag{1}$$

Shockley's diode current equation is a basic mathematical formula that explains I–V, the properties of a photovoltaic solar cell, or Equation (2). It is derived from semiconductor theory.

$$I_d = I_s \left[exp \left(\frac{qV_{oc}}{N_S K A T_0} \right) - 1 \right] \tag{2}$$

The resulting current I of a model solar cell is produced by entering the value of the I_d in Equation (1), as shown in Equation (3).

$$I = Iph - I_s \left[exp \left(\frac{qV_{oc}}{N_S K A T_0} \right) - 1 \right] \tag{3}$$

A solar cell's ideal photon-produced current is directly related to both illumination intensity and irradiance and is approximated very well. The output of PV is influenced by some parameters that are not included in the ideal case model. The modified single-diode model for the actual case is shown in the following subsection.

3.2. Operation of Modified SEPIC Converter

There are two modes of operation for the modified SEPIC converter topology: closed and open. Analyzing the converter's operating mode involves looking at how each component behaves in a steady state. The inductor currents, I_{L1} and I_{L2}, are always continuous when the converter is operating in Continuous Conduction Mode (CCM), which lasts for one switching period. It is also expected that the capacitor's voltage will not change.

This part defines the presentation of the modified SEPIC converter shown in Figure 3(a), which combines a Boost converter and Buck converter. Converter enabled with three indicators. L_1, L_2 and L_3, two capacitors C_1, C_2 and load resistance R_L. The operation of a modified SEPIC converter is defined as follows. When switch S_1 is closed, current flows through the inductor L_1 increases. Diode D_1, D_2 is counter-polarized, and C_1 generates energy to the output stage. The current through L_2 also increases while the voltage across C_1 decreases, as shown in Figure 3(b).
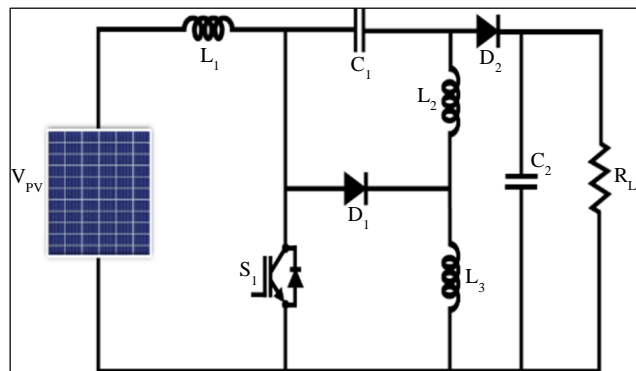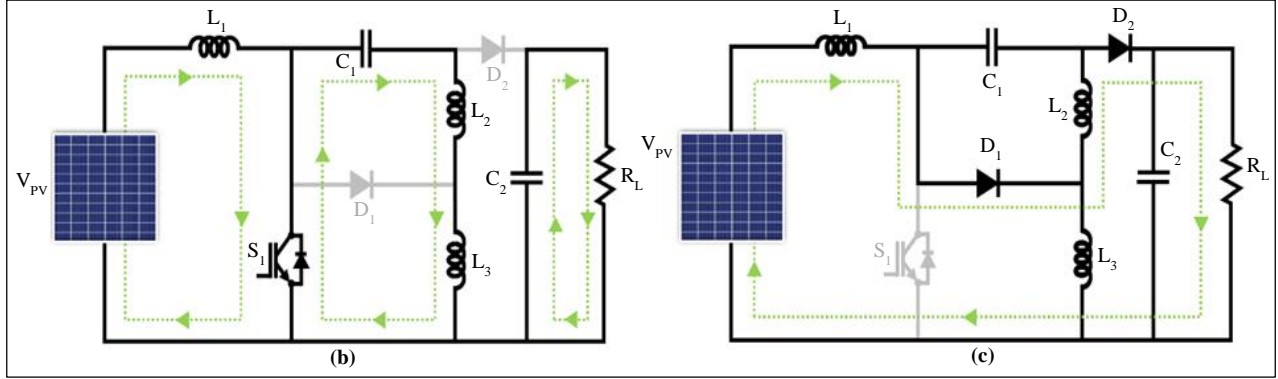

(a)

Fig. 3 Proposed converter (a) Equivalent circuit, (b) Operation at mode-I, and (c) Operation at mode-II.

$$V_{pv} = V_{in} \tag{4}$$

$$V_{pv} = V_{L1} \tag{5}$$

$$V_{pv} = L_1 \frac{dI_{L1}}{dt} \tag{6}$$

$$V_{pv} = L_1 \frac{\Delta I_{L1}}{t_{on}} \tag{7}$$

It is necessary for voltage across inductor L_3 to equal the total of voltages across the capacitor C_1 and inductor L_2. After that, the formula becomes:

$$V_{L3} = V_{L2on} + V_{C1} \tag{8}$$

$$V_{L3} - L_2 \frac{dI_{L2}}{dt} - V_{C1} \tag{9}$$

$$V_{L3} = L_2 \frac{\Delta I_{L2}}{t_{on}} + V_{C1} \tag{10}$$

The voltage across the resistor L_1 and input voltage added together equals the voltage on the inductor L_3 while the switch is open, shown in Figure 3(c), giving us the following equation:

$$V_{L3} = V_{in} + V_{L1off} \tag{11}$$

$$V_{L3} = V_{in} + L_1 \frac{dI_{L1}}{dt} \tag{12}$$

$$V_{L3} - V_{in} + L_1 \frac{\Delta I_{L1}}{t_{off}} \tag{13}$$

A voltage equivalent to the voltage of the V_{C1} must be applied across the inductor L_2. And the following explanation applies:

$$V_{C1} = V_{L2} \tag{14}$$

$$V_{C1} = L_2 \frac{dI_{L2}}{dt} \tag{15}$$

$$V_{C1} = L_2 \frac{\Delta I_{L2}}{t_{off}} \tag{16}$$

$$V_{C1} \cdot t_{off} = L_2 \cdot \Delta I_{L2} \tag{17}$$

Furthermore, the output voltage V_0, is represented by the following equation, will be equal to the sum of voltages across inductor L_2 and L_3 while the switch is open.

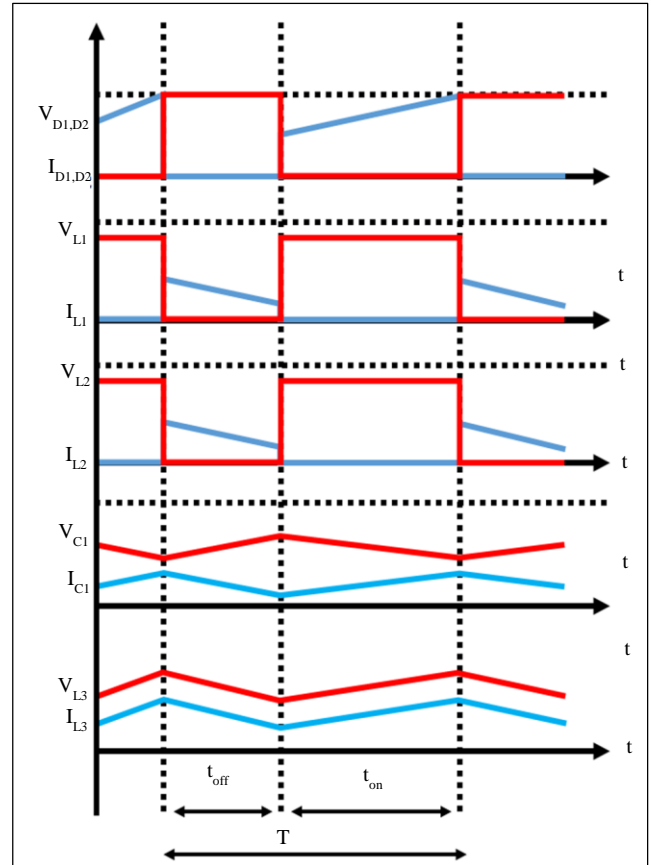$$V_0 = V_{C1} + V_{L3} \tag{18}$$

Fig. 4 Waveform of switching characteristics of converter

The following equation was produced by replacing Equation 7 in Equation 13:

$$V_{L3} = \left(\frac{1}{1-D}\right) V_{in} \tag{19}$$

$$\frac{V_{L3}}{V_{in}} = \left(\frac{1}{1-D}\right) \tag{20}$$

Equation 11 was then substituted into Equation 7, yielding the subsequent equation:

$$V_{L3} = \left(\frac{1}{D}\right) V_{C1} \tag{21}$$

Equation 21 changed to Equation 15, which produced the following equation:

$$\frac{V_{L3}}{V_{in}} = \left(\frac{D}{1-D}\right) \tag{22}$$

The output voltage should match the total of the voltages on the capacitors. C_1 and L_3, according to Equation 12. The following equation was found by replacing Equations 17 and 15 in Equation 12:

$$V_0 = \left(\frac{1+D}{1-D}\right) V_{in} \tag{23}$$

$$\frac{V_0}{V_{in}} = \left(\frac{1-D}{1-D}\right) \tag{24}$$

The modified SEPIC converter topology's conversion rate can be found using Equation 24. The duty cycle, which has a value in the range of 0 to 1, determines the output voltage. The converter's output voltage increases with increasing duty cycle.

3.3. Artificial Neural Network-Based MPPT Technique

ANNs have proven to be effective in various domains by providing precise and swifter solutions for intricate mathematical models. Because ANNs respond quickly and accurately to a variety of environmental variables, they are employed in the MPPT system. A variety of activation functions are available for use. The following equations are used to express a neuron's output:

$$v_k = \sum_{x=1}^{x=n} (w_{ki} \cdot x_i + b) \tag{25}$$

$$y_k = f(-v_k) \tag{26}$$

Where, for neuron k, x_i is the ith input, and y_k is the output, w_{ki} is a weight from input i to neuron k, b is the bias, f is the activation function.

Figure 4 depicts an overview of the ANN utilized for MPPT, with G and Tc serving as the conventional inputs. The duty cycle (D) output signal is used to modify PV voltage via a converter.
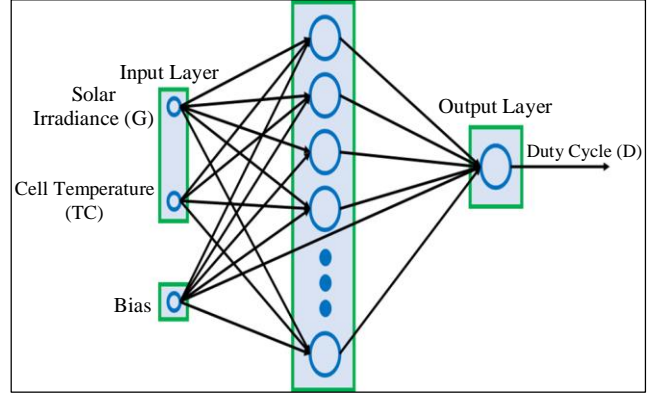

Fig. 5 The ANN architecture for MPPT

In order to track maximum output power, ANN is employed as a control system to instruct D to modify. V_{pv} Via boost converter. The relationship between PV array voltage (V_{pv}), duty cycle (D), and inverter's dc voltage (V_{dc}) is shown as follows:

$$V_{pv} = (1 - D * V_{dc}) \tag{27}$$

The PV model described in Section II provides the training data (i.e., targets and inputs) needed to train the ANN for MPPT. The trained ANN can be employed for MPPT once a certain performance is attained, as determined by the Mean Square Error (MSE). Figure 6 is a flowchart that explains the ANN's training process technique for MPPT.
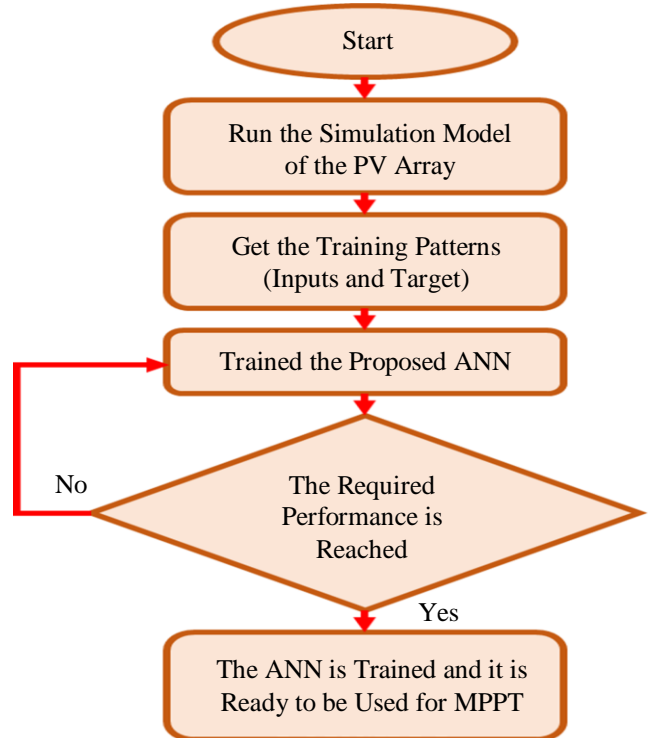

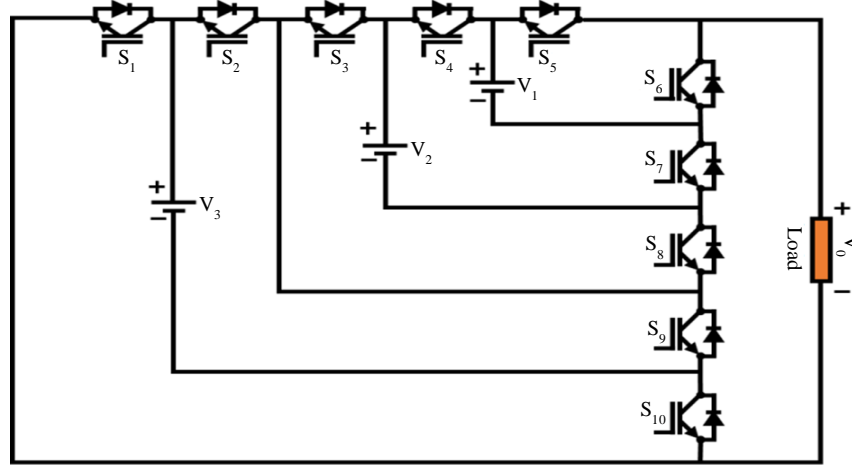**Fig. 6 A flowchart of the training process of the ANN for MPPT**

Fig. 7 Proposed 21-level MLI

Table 1. Switching operations for the proposed 21-level MLI

Levels	S_1	S_2	S_3	S_4	S_5	S_6	S_7	S_8	S_9	S_{10}
Level-1	0	1	1	0	1	0	1	0	0	1
Level-2	0	1	1	0	0	1	1	0	0	1
Level-3	0	1	0	0	1	0	1	1	0	1
Level-4	0	1	1	1	1	0	0	0	0	1
Level-5	0	1	1	1	0	1	0	0	0	1
Level-6	1	0	1	0	0	1	1	0	1	0
Level-7	0	1	0	1	0	1	0	1	0	1
Level-8	0	0	1	0	1	0	1	0	1	1
Level-9	0	0	1	0	0	1	1	0	1	1
Level-10	0	0	0	0	1	0	1	1	1	1
Level-11	0	0	0	0	0	1	1	1	1	1
Level-12	0	0	0	0	1	0	1	1	1	1
Level-13	0	0	1	0	0	1	1	0	1	1
Level-14	0	0	1	0	1	0	1	0	1	1
Level-15	0	1	0	1	0	1	0	1	0	1
Level-16	1	0	1	0	0	1	1	0	1	0
Level-17	0	1	1	1	0	1	0	0	0	1
Level-18	0	1	0	1	1	0	0	0	0	1
Level-19	0	1	1	0	1	0	1	1	0	1
Level-20	0	1	1	0	0	1	1	0	0	1
Level-21	0	1	1	0	1	0	1	0	0	1

3.4. Reduced Switch 21-Level MLI

The proposed innovative asymmetrical 21-level MLI, illustrated in Figure 7, has fewer components. DC sources and 10 controlled switches make up the recommended MLI configuration. Many power quality concerns are reduced by the MLI architecture, such as cost factor, Total Standing Voltage (TSV) cost per unit with varying weight factor values, THD, switch count, number of components, and voltage stress. This topology is compared with other topologies and yields lower TSV.

The function of switches allows one to observe the proposed 21-level MLI through the switching pulses. The switch is in the "1" state when it is turned on; otherwise, it is in the "0" state. The switches generate an output voltage of 400V and function in multiple modes. Three voltages of

varying magnitudes (V_1, V_2 and V_3) are included in the design of the MLI. The $1:2:7$ ratio is used to select these voltages. Hence, the voltages are therefore $40V, 80V,$ and $280V$, respectively. As a result, an output voltage of $400V$ is obtained using a 100Ω resistor and a $4A$ current.

3.5. Chaotic PSO-Proportional Resonant Controller

A system with a PR current controller can be shown using the block diagram displayed in Figure 8 below. The picture essentially depicts three block systems: the blocks for the controller, inverter, and filter.

The output current Ii will be compared to the current reference, $I_i *$ after the filtering process, the controlling system receives the resulting error as input. The PR current controller $G_{PR}(S)$ is depicted in the diagram as follows:

$$G_{PR}(S) = K_P + K_I \frac{S}{S^2 + \omega_0^2} \tag{28}$$

Where ω_0 the resonant frequency, K_I is the integral gain term, and K_P is the proportional gain term. Since the resonant term at the system frequency will essentially yield infinite gain, there won't be any phase shift or gain at other frequencies, ω_0.

The gain, phase, and bandwidth of the system are all under the control of the K_P term. Despite all of this, the unlimited gain in (28) may produce stability issues. It is, therefore, possible to make the control system less than optimal. Damping is introduced in order for this to occur. It is displayed in (29) below.

$$G_{PR}(S) = K_P + K_I \frac{2\omega_c s}{S^2 + 2\omega_c s + \omega_0^2} \tag{29}$$

Where, ω_c is the bandwidth surrounding the ω_0 system frequency. The equation now sets a limit on the controller's gain at the system frequency ω_0. However, it is still significant enough to cause very little steady-state error.

3.5.1. Chaos Particle Swarm Optimization Algorithm

Particle i s position in a D-dimensional search space is represented by $X_i^t = (X_{i1}^t, X_{i2}^t, \cdots, X_{iD}^t)^T$, and its velocity is represented by $V_i^t = (V_{i1}^t, V_{i2}^t, \cdots, V_{iD}^t)^T$. P_{best} represents the best prior fitness and matching position of particle i while $P_i^t = (P_{i1}^t, P_{i2}^t, \cdots, P_{iD}^t)^T$ represents the comparable position.

The best particle's fitness and location within the swarm are denoted by g_{best} and $P_g^t = (P_{g1}^t, P_{g2}^t, \cdots, P_{gD}^t)^T$. The search procedure in the typical PSO can be stated as follows:

$$V_{id}^t = wV_{id}^{t-1} + c_1 r_1 + (P_{id}^{t-1} - x_{id}^{t-1}) + c_2 r_2 + \left(P_{gd}^{t-1} - x_{id}^{t-1}\right) \tag{30}$$

$$x_{id}^t = x_{id}^{t-1} + V_{id}^t \tag{31}$$

Where r_1 and r_2 are uniformly distributed random values with a range of $(0, 1)$, t is the sum of iterations, w is the inertia weight, c_1 and c_2 are the cognitive and social acceleration coefficients, respectively.

An evaluation function is chosen in the PSO method to determine the position quality of the particles. In the study, the fitness function is specified as the Integrated Time and Absolute Error (ITAE), which is utilized as follows:

$$F = \int_0^1 t|e(t)|d(t) \tag{32}$$

A standard chaotic system is the logistic equation,

$$Z(t + 1) = \mu z(t)[1 - z(t)] \tag{33}$$

Where, $z \in [0, 1](z(0) \neq 0, 0.25, 0.50, 0.75, 1), \mu$ is the control parameter.

Chaos initialization can increase the quantity and quality of initial particles produced during particle swarm initialization by producing a high number of organized chaotic particles. In order to address the issue of particles being readily imprisoned in the local extremum of the PSO algorithm, chaos disruption is incorporated into the search process, causing particles to leap out of the local extremum and achieve global optimization.

The two significant components of chaos theory are chaos disturbance and chaos initialization. The CPSO procedure is as follows:

1. The initial groups are chosen using the fitness-best selection principle, and the particle's position and velocity are initialized with the chaos.
2. To create a new particle, add a disturbance Δx to each particle's current position. To create a new particle group, compare the fitness values of the latest and old particles and choose the particle that performs better.
3. To get the matching particle, update both the global and individual extrema.
4. Adjust the particle's velocity and position based on expressions (30) and (31).
5. Find the convergence condition. The best feasible solution is generated, and the iteration finishes when the termination condition is satisfied.
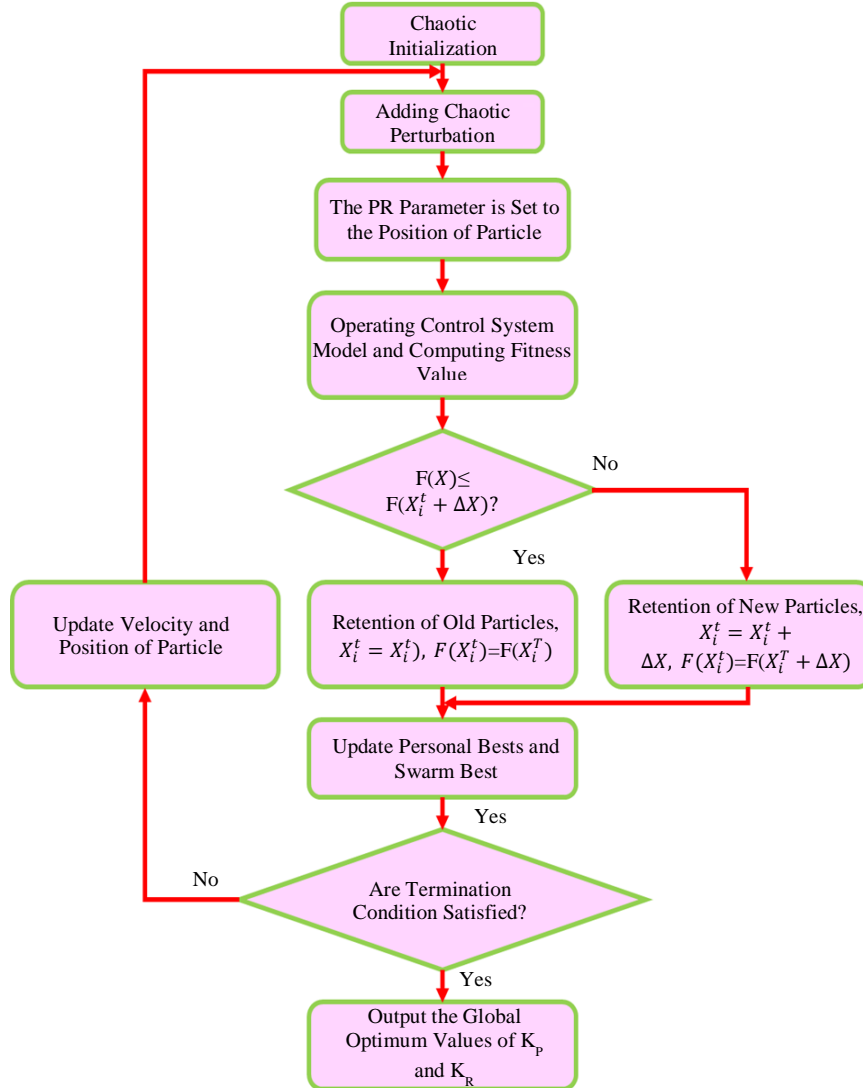
Fig. 8 The process of tuning the PR parameters using the CPSO algorithm

4. Results and Discussion

An in-depth examination of the proposed system using an ANN-based MPPT system integrated with Modified SEPIC converter outputs will be covered in this section, along with essential metrics, including converter efficiency, voltage stability, and the overall efficacy of the recommended control technique.

A unique strategy investigated in this research is the incorporation of a Chaotic PSO-PR controller into the Reduced Switch 21 level MLI to provide optimal performance. Using MATLAB, a proposed system's full simulation is verified, and the system's functionality is investigated. It is assumed that the corresponding constant temperature and irradiation values of $35°C$ and $1000\,W/Sq$ are obtained based on the observation of the solar panel temperature and irradiation illustrated in Figure 9.

Table 2. Specification of parameters

Parameter	Rating
Solar PV System	
Series Connected Solar PV Cells	36
Total Power	10KW
Peak Power	150W
Open Circuit Voltage	37.25V
Short Circuit Current	8.95A
Modified SEPIC Converter	
L_1, L_2, L_3	1mH
C_1, C_2	4.7μF
C_o	2200μF
Switching Frequency	10kHz

Figure 10 illustrates the waveform representation of the solar panel's current and voltage, from which a constant voltage of 70V is determined. Similarly, the current is settled at 5A after 0.3s.

It is observed that at the beginning, the converter output voltage's waveform rises to 400v to 700V and shows settlement at $0.2s$ with a stabilized voltage value of 690V, as depicted in Figure 11(a). Simultaneously, in Figure 11(b), the output current waveform of the converter rises at the initial stage and sustains at 6A at 0.2 seconds and then remains constant.

In Figure 12, four different input voltage waveforms are observed for DC voltage flows through when it enters the reduced switch 21 level MLI. The power source outputs at a variety of waveforms, including 69V, 130V, 270V, and 550V all without any time variation of $0.2s$ with random variations.
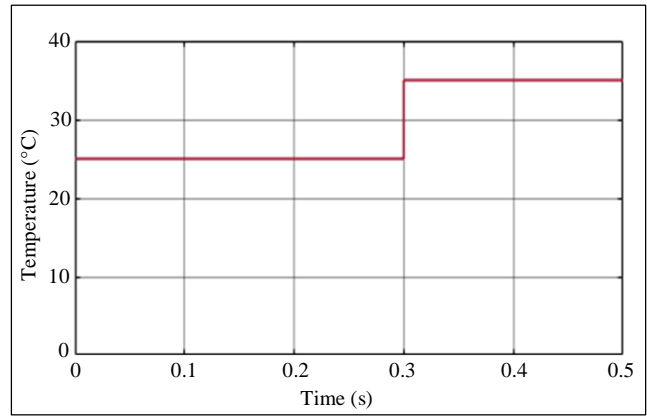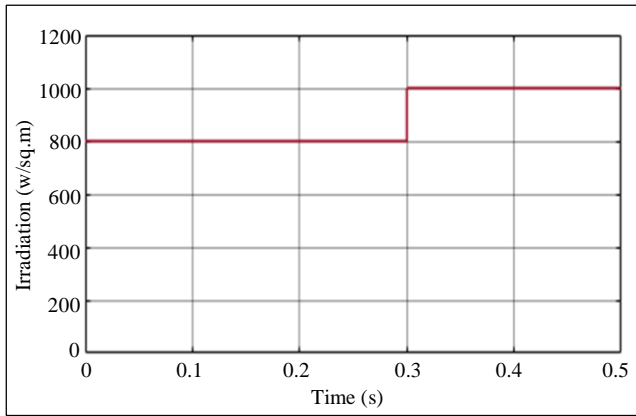
Fig. 9 Solar panel irradiance and temperature waveform
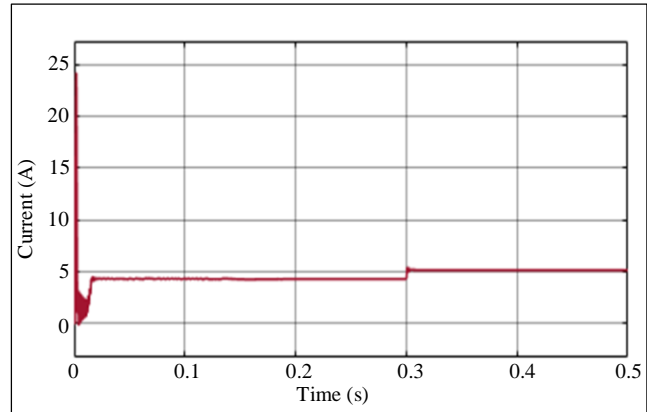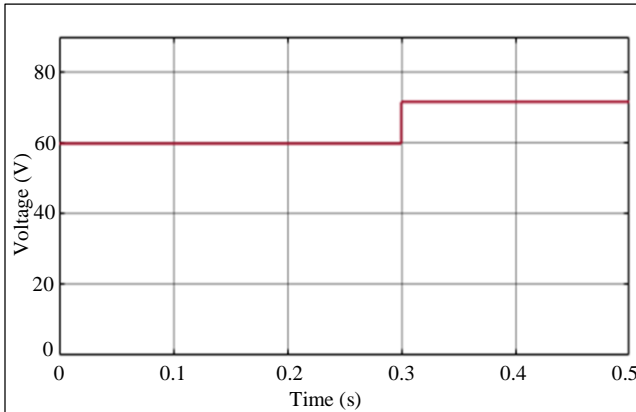
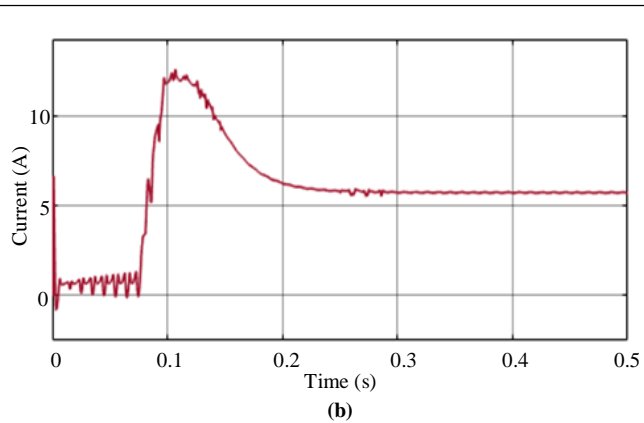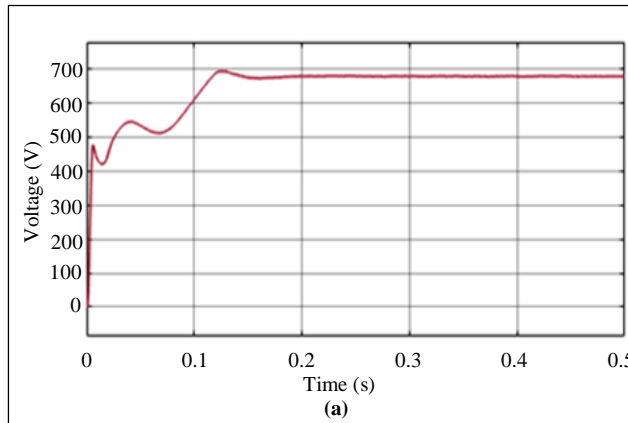
Fig. 10 Solar panel voltage and current waveform

Fig. 11 Converter output (a) Voltage, and (b) Current waveform.
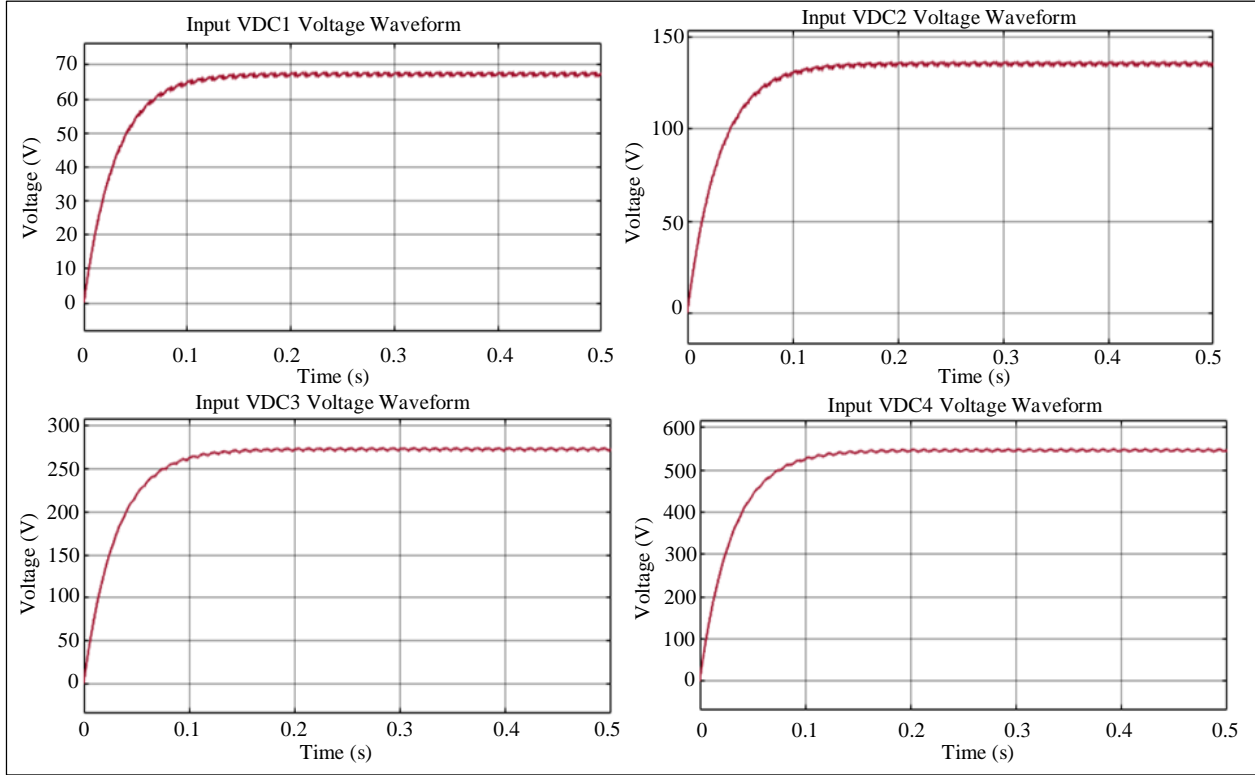
Fig. 12 Input VDC voltage waveform

The output voltage response of 21-level MLI is illustrated in Figure 13(a). It is observed that a stabilized inverter voltage of $650V$ is accomplished, which is maintained without any further distortions.

Similarly, in Figure 13(b), the output current response of 21-level MLI is illustrated; there are no more distortions noticed, and an inverter current of $13A$ is observed to be stable. The outcomes proposed 3φ grid voltage and current illustrated in Figure 14. It is noticed that a stabilized grid voltage of $415V$ is accomplished, followed by a grid current of $12A$ is attained, showcasing the enhanced grid performance of the proposed system.

In Figure 15, the in-phase grid voltage waveform represents the sinusoidal voltage supplied by the electrical grid, with its peaks and zero crossings aligned with those of the in-phase grid current waveform. This alignment signifies an ideal scenario where the voltage and current are in phase with each other, a condition conducive to efficient power transfer.

In Figure 16, the power factor waveform displays a gradual increase until it reaches a steady state level of 1 per unit (1 PU). The gradual rise observed in the power factor waveform suggests a dynamic process where the system is adjusting and optimizing its power factor over time.
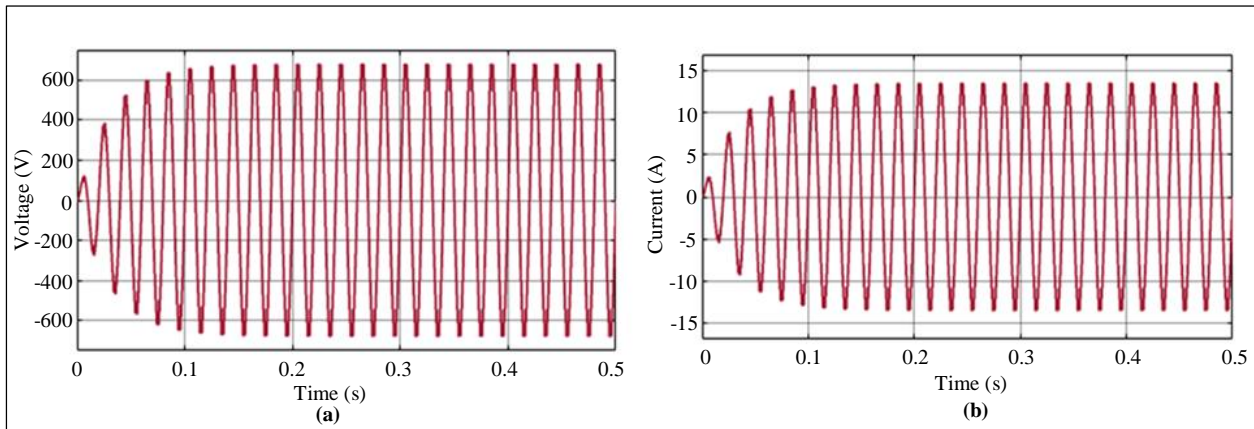

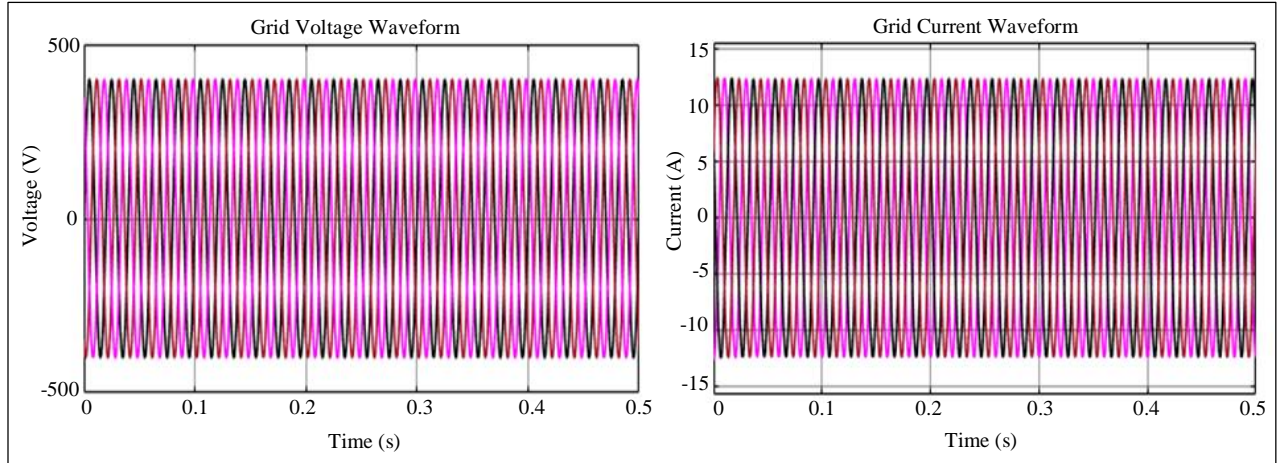**Fig. 13 Output (a) Voltage, and (b) Current waveforms of proposed reduced switched 21-level MLI.**

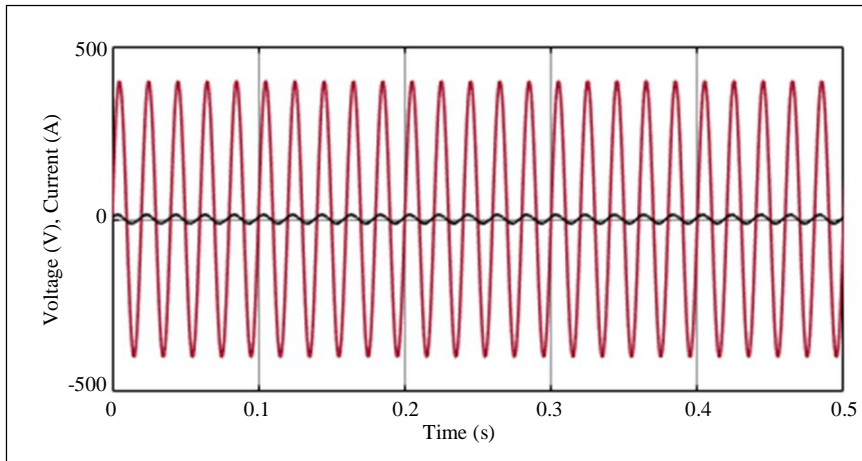**Fig. 14 Grid voltage and current waveform**

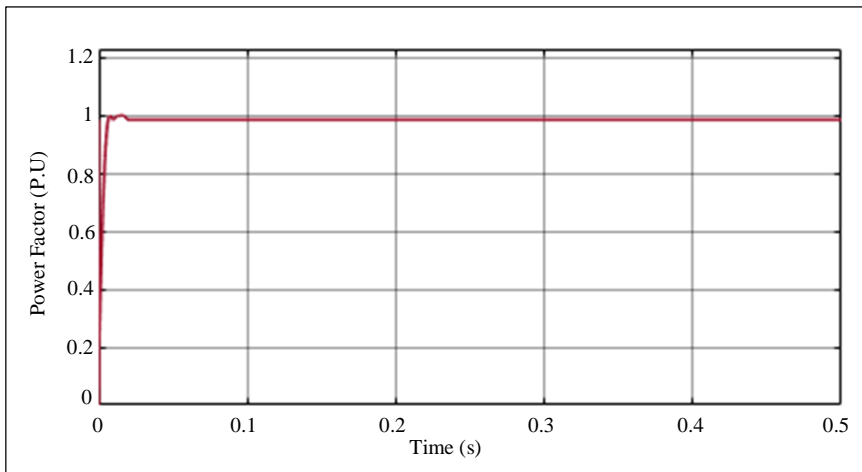**Fig. 15 In-phase grid voltage and current waveform**

Fig. 16 Power factor waveform

The waveforms for reactive and real power are shown in Figure 17. Reductions in reactive power in this context lead to improved actual power performance because they make it possible for the system to use active power more effectively, improving total power efficiency. The waveform in Figure 18 shows the existence of harmonic distortion with a THD value of 2.54%. As can be seen from the figure, more sinusoidal waveforms are indicated by a lower THD value.

The provided comparison in Figure 19 offers a glimpse into the efficiencies of different converters. Firstly, the SEPIC [17] demonstrates an efficiency of 88.82%, showcasing its capability to convert input power with a high level of effectiveness. Following this, Luo [18] exhibits a slightly higher efficiency of 90%, which is somewhat more efficient than the standard SEPIC. Finally, the proposed Modified SEPIC stands out with an efficiency of 92.01%, denoting a notably higher conversion efficiency in contrast to other converters.
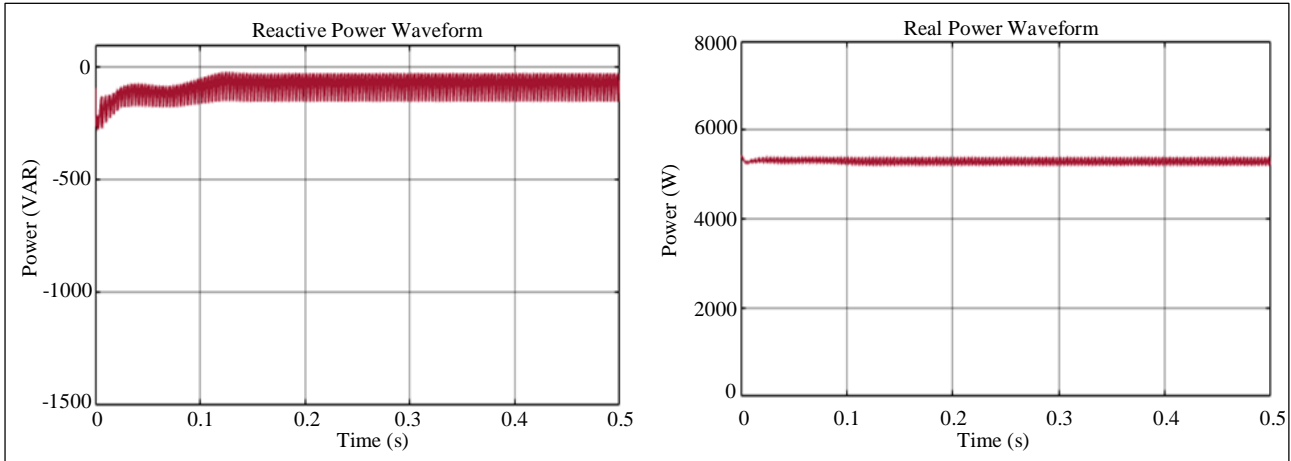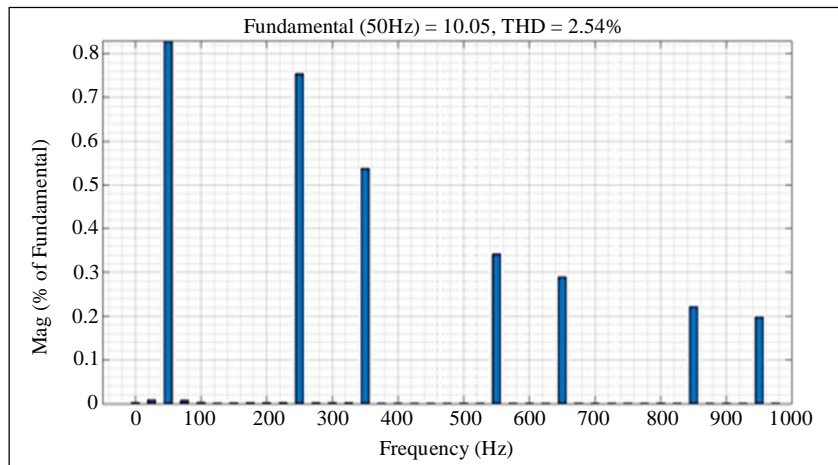

Fig. 17 Reactive and real power waveform
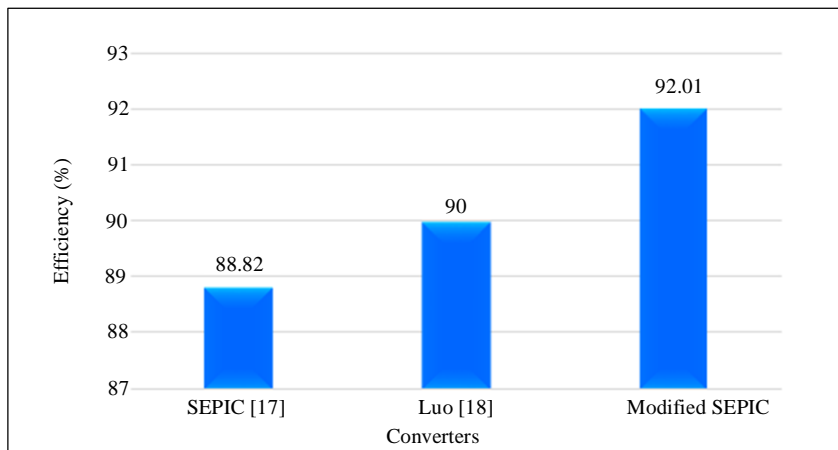

Fig. 18 Grid current THD waveform

Fig. 19 Comparison of converter efficiency

Table 3. Comparison of THD analysis

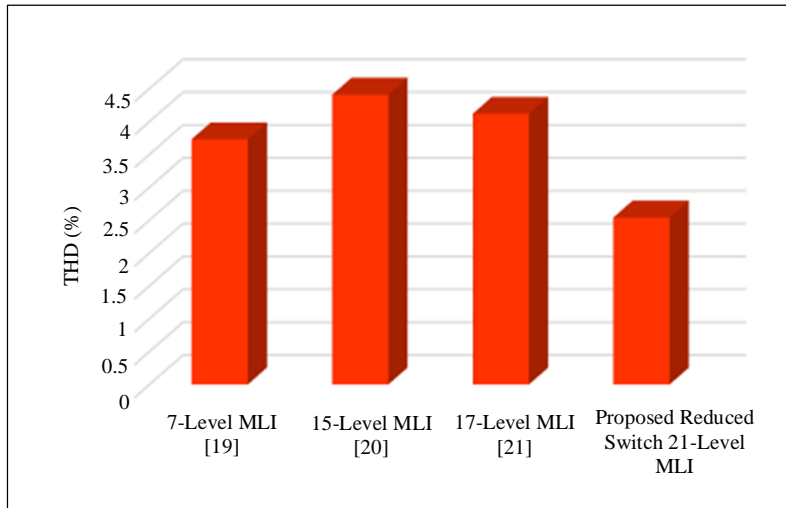| MLI Topologies	THD (%)
7-Level MLI [19]	3.73
15-Level MLI [20]	4.41
17-Level MLI [21]	4.12
Proposed Reduced Switch 21-Level MLI	2.54

Fig. 20 THD Performance analysis

This THD comparison for various MLI topologies is listed in Table 3, with its graphical representation in Figure 20. The 7-Level MLI shows a THD of 3.73%, indicating a relatively clean output waveform. The 15-level MLI and 17-level MLI exhibit slightly higher THD values at 4.41% and 4.12%, respectively, suggesting a somewhat increased level of harmonic distortion. In contrast, a Proposed Reduced Switch 21-level MLI stands out with a lower THD of 2.54%, indicating a more efficient and cleaner output waveform, likely due to innovative modifications.

The comparison chart in Figure 21 presents various MPPT techniques alongside their associated tracking efficiencies. The variable step size P&O [22] achieves a tracking efficiency of 95.40%, while the incremental conductance achieves a slightly lower tracking efficiency of 95%. Meanwhile, the Variable Step size incremental conductance achieves a slightly lower efficiency of 94.77%. It is observed that the proposed ANN-based MPPT stands out with a high tracking efficiency of 98.82%, indicating precise and efficient power point tracking.

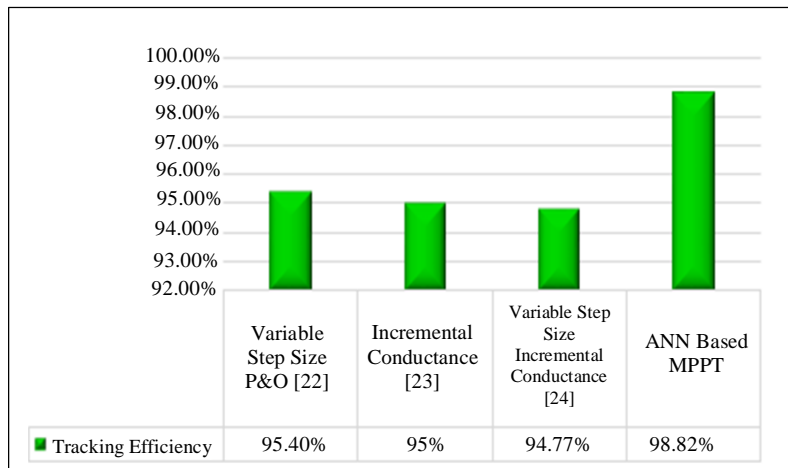|	Variable Step Size P&O [22]	Incremental Conductance [23]	Variable Step Size Incremental Conductance [24]	ANN Based MPPT
■ Tracking Efficiency	95.40%	95%	94.77%	98.82%

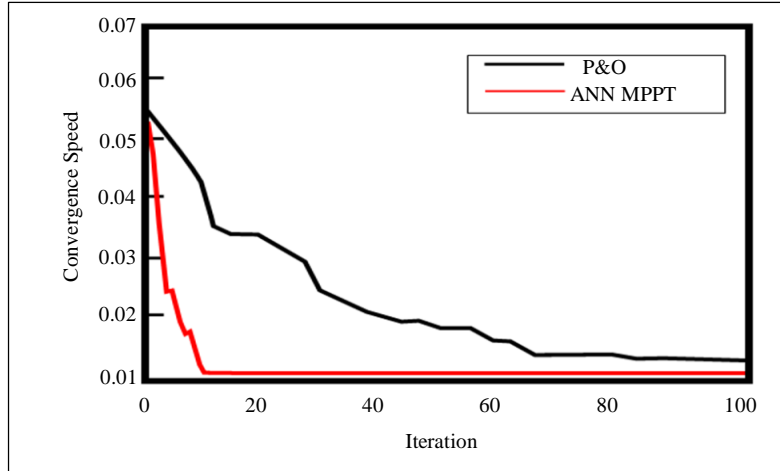**Fig. 21 Comparison of tracking efficiency**

Fig. 22 Comparison of convergence speed

The comparison of convergence speed is illustrated in Figure 22, comparing the proposed ANN-MPPT with conventional MPPT approaches. From the figure, it is analyzed that the proposed ANN approach shows faster convergence, in contrast to other methods.

5. Conclusion

This paper addresses the imperative need for a diversified energy mix to meet the growing demand for electricity by introducing the ANN- technique to track optimal power out of PV. Additionally, the paper proposes the use of a modified SEPIC to boost voltage from PV sources. The integration of a Reduced Switch 21-level MLI is employed to convert DC output from PV modules into AC with an increased number of output levels compatible with the grid. To ensure precise control and efficient grid synchronization, a chaotic PSO-PR controller is implemented. The validation outcomes show that the proposed converters rank with an improved efficiency of 92.01%, with enhanced voltage gain.

Moreover, the proposed MLI results with reduced THD of 2.54%, displaying minimized harmonics. Furthermore, the developed MPPT techniques resulted in a significantly higher tracking efficiency of 98.82%. This comprehensive approach not only maximizes the utilization of solar energy but also enhances the entire performance of the PV system.

References

[1] Cagfer Yanarates, and Zhongfu Zhou, "Symmetrical Pole Placement Method-Based Unity Proportional Gain Resonant and Gain Scheduled Proportional (PR-P) Controller with Harmonic Compensator for Single Phase Grid-Connected PV Inverters," *IEEE Access*, vol. 9, pp. 93165-93181, 2021. [CrossRef] [Google Scholar] [Publisher Link]

[2] Viswaprakash Babu et al., "Power Quality Enhancement Using Dynamic Voltage Restorer (DVR)-Based Predictive Space Vector Transformation (PSVT) with Proportional Resonant (PR)-Controller," *IEEE Access*, vol. 9, pp. 155380-155392, 2021. [CrossRef] [Google Scholar] [Publisher Link]

[3] Shubhra Shubhra, and Bhim Singh, "Three-Phase Grid-Interactive Solar PV-Battery Microgrid Control Based on Normalized Gradient Adaptive Regularization Factor Neural Filter," *IEEE Transactions on Industrial Informatics*, vol. 16, no. 4, pp. 2301-2314, 2020. [CrossRef] [Google Scholar] [Publisher Link]

[4] A.M. Mahfuz-Ur-Rahman et al., "An Advanced Modulation Technique for Transformerless Grid Connected Inverter Circuits Used in Solar Photovoltaic Systems," *IEEE Transactions on Industrial Electronics*, vol. 70, no. 4, pp. 3878-3887, 2023. [CrossRef] [Google Scholar] [Publisher Link]

[5] Sivanagaraju Gangavarapu, Manish Verma, and Akshay Kumar Rathore, "A Novel Transformerless Single-Stage Grid-Connected Solar Inverter," *IEEE Journal of Emerging and Selected Topics in Power Electronics*, vol. 11, no. 1, pp. 970-980, 2023. [CrossRef] [Google Scholar] [Publisher Link]

[6] K.S. Kavin, and P. Subha Karuvelam, "PV-Based Grid Interactive PMBLDC Electric Vehicle with High Gain Interleaved DC-DC SEPIC Converter," *IETE Journal of Research*, vol. 69, no. 7, pp. 4791-4805, 2023. [CrossRef] [Google Scholar] [Publisher Link]

[7] Ali Faisal Murtaza et al., "Efficient MPP Tracking of Photovoltaic (PV) Array through Modified Boost Converter with Simple SMC Voltage Regulator," *IEEE Transactions on Sustainable Energy*, vol. 13, no. 3, pp. 1790-1801, 2022. [CrossRef] [Google Scholar] [Publisher Link]

[8]   Amresh Kumar Singh, Shailendra Kumar, and Bhim Singh, "Solar PV Energy Generation System Interfaced to Three Phase Grid With Improved Power Quality," *IEEE Transactions on Industrial Electronics*, vol. 67, no. 5, pp. 3798-3808, 2020. [CrossRef] [Google Scholar] [Publisher Link]

[9]   Kaibalya Prasad Panda, Sze Sing Lee, and Gayadhar Panda, "Reduced Switch Cascaded Multilevel Inverter with New Selective Harmonic Elimination Control for Standalone Renewable Energy System," *IEEE Transactions on Industry Applications*, vol. 55, no. 6, pp. 7561-7574, 2019. [CrossRef] [Google Scholar] [Publisher Link]

[10]   Prabhat Ranjan Bana et al., "Recently Developed Reduced Switch Multilevel Inverter for Renewable Energy Integration and Drives Application: Topologies, Comprehensive Analysis and Comparative Evaluation," *IEEE Access*, vol. 7, pp. 54888-54909, 2019. [CrossRef] [Google Scholar] [Publisher Link]

[11]   Ali Hajjiah Chaoping Rao et al., "A Novel High-Gain Soft-Switching DC-DC Converter with Improved P&O MPPT for Photovoltaic Applications," *IEEE Access*, vol. 9, pp. 58790-58806, 2021. [CrossRef] [Google Scholar] [Publisher Link]

[12]   Ankur Kumar Gupta et al., "Effect of Various Incremental Conductance MPPT Methods on the Charging of Battery Load Feed by Solar Panel," *IEEE Access*, vol. 9, pp. 90977-90988, 2021. [CrossRef] [Google Scholar] [Publisher Link]

[13]   Tole Sutikno, Arsyad Cahya Subrata, and Ahmad Elkhateb, "Evaluation of Fuzzy Membership Function Effects for Maximum Power Point Tracking Technique of Photovoltaic System," *IEEE Access*, vol. 9, pp. 109157-109165, 2021. [CrossRef] [Google Scholar] [Publisher Link]

[14]   Bushra Sabir et al., "A Novel Isolated Intelligent Adjustable Buck-Boost Converter with Hill Climbing MPPT Algorithm for Solar Power Systems," *Processes*, vol. 11, no. 4, pp. 1-23, 2023. [CrossRef] [Google Scholar] [Publisher Link]

[15]   Shaik Reddi Khasim et al., "A Novel Asymmetrical 21-Level Inverter for Solar PV Energy System with Reduced Switch Count," *IEEE Access*, vol. 9, pp. 11761-11775, 2021. [CrossRef] [Google Scholar] [Publisher Link]

[16]   Venu Sonti, Sachin Jain, and Bhagya Sai Kumar Reddy Pothu, "Leakage Current Minimization Using NPC DC Decoupling Method for Three-Phase Cascaded Multilevel PV Inverter," *IEEE Transactions on Circuits and Systems II: Express Briefs*, vol. 67, no. 12, pp. 3247-3251, 2020. [CrossRef] [Google Scholar] [Publisher Link]

[17]   Patan Javeed et al., "SEPIC Converter for Low Power LED Applications," *Journal of Physics: Conference Series*, vol. 1818, 2021. [CrossRef] [Google Scholar] [Publisher Link]

[18]   S. Sivarajeswari, and D. Kirubakaran, "Design and Development of Efficient Luo Converters for DC Micro Grid," *The International Journal of Electrical Engineering & Education*, vol. 60, no. 1, 2019. [CrossRef] [Google Scholar] [Publisher Link]

[19]   Ahmed Ismail M. Ali, Mahmoud A. Sayed, and Ahmed A. S. Mohamed, "Seven-Level Inverter with Reduced Switches for PV System Supporting Home-Grid and EV Charger," *Energies*, vol. 14, no. 9, pp. 1-23, 2021. [CrossRef] [Google Scholar] [Publisher Link]

[20]   C. Dhanamjayulu et al., "Design and Implementation of a Single-Phase 15-Level Inverter with Reduced Components for Solar PV Applications," *IEEE Access*, vol. 9, pp. 581-594, 2021. [CrossRef] [Google Scholar] [Publisher Link]

[21]   C. Dhanamjayulu et al., "Design and Implementation of Seventeen Level Inverter with Reduced Components," *IEEE Access*, vol. 9, pp. 16746-16760, 2021. [CrossRef] [Google Scholar] [Publisher Link]

[22]   Ahmed I.M. Ali, Mahmoud A. Sayed, and Essam E.M. Mohamed, "Modified Efficient Perturb and Observe Maximum Power Point Tracking Technique for Grid-Tied PV System," *International Journal of Electrical Power & Energy Systems*, vol. 99, pp. 192-202, 2018. [CrossRef] [Google Scholar] [Publisher Link]

[23]   Nur Fairuz Mohamed Yusof, Dahaman Ishak, and Mohamed Salem, "An Improved Control Strategy for Single-Phase Single-Stage Grid-Tied PV System Based on Incremental Conductance MPPT, Modified PQ Theory, and Hysteresis Current Control," *Engineering Proceedings*, vol. 12, no. 1, pp. 1-4, 2022. [CrossRef] [Google Scholar] [Publisher Link]

[24]   Adeel Feroz Mirza et al., "Advanced Variable Step Size Incremental Conductance MPPT for a Standalone PV System Utilizing a GA-Tuned PID Controller," *Energies*, vol. 13, no. 16, pp. 1-24, 2020. [CrossRef] [Google Scholar] [Publisher Link]